A Sample/Jitter Monte Carlo Technique for Main Parachute Loads Predictions

Eric S. Ray[1] and Leonard D. Cassady Ph.D.[2]
National Aeronautics and Space Administration, Johnson Space Center, Houston, TX, 77058

John Y. Davidson[3]
GeoControl Systems, Inc., Houston, TX, 77054

Models for Orion parachute performance are based on reconstructions of the Capsule Parachute Assembly System (CPAS) drop test campaign and were documented in the CPAS "Model Memo." Experience with similar Commercial Crew Program (CCP) parachute systems resulted in some updates to the Orion models in preparation for Artemis missions. The reefing cutter dispersion model for the drogues and mains had been overly-conservative by producing wide timing differences within clusters. A higher-fidelity timing model was generated by separating out in-lot variation and temperature effects. The main parachute inflation model had accounted for some correlations between parameters using complicated 2-D geometric bounding, but the results tended to exaggerate individual peak loads from fast (leading) inflations and under-emphasize actual lagging experience. Several flight tests were reconstructed again with an emphasis on matching peak load magnitudes using a search algorithm. A simpler method for generating inflation parameters uses the 3-D correlated reconstructed "samples" with some random "jitter" applied. Dispersed Monte Carlo inputs are then checked against flight test data to evaluate whether they represent reality.

Nomenclature

CCP	=	Commercial Crew Program
$(C_DS)(t)$	=	Drag area growth as a function of time
$(C_DS)_{i-1}$	=	Drag area at the end of previous stage
$(C_DS)_i$	=	Drag area at the end of stage i
$(C_DS)_o$	=	Full open drag area
$(C_DS)_{p,i}$	=	Dynamic drag area of individual parachute i
CDT	=	Cluster Development Test (series)
CPAS	=	Capsule Parachute Assembly System
CQT	=	Cluster Qualification Test (series)
DLAT	=	Destructive Lot Acceptance Test (for reefing cutters)
D_o	=	Nominal parachute diameter based on reference area, $D_o = \sqrt{4 \cdot S_o / \pi}$
EDU	=	Engineering Development Unit (test series)
expopen	=	Opening profile shape exponent: < 1.0 concave down; = 1.0 linear; > 1.0 concave up
FBCP	=	Forward Bay Cover Parachute
F	=	Tension force in a parachute riser
g	=	Acceleration of Earth Gravity
G	=	Load factor (dimensionless)
MPCV	=	Multi-Purpose Crew Vehicle (Orion)
n	=	Canopy filling constant, normalized to reference diameter

[1] Analysis Engineer, Aeroscience Branch, NASA Johnson Space Center/EG3, AIAA Senior Member.
[2] Analysis Engineer, Aeroscience Branch, NASA Johnson Space Center/EG3, AIAA Member.
[3] Analysis Engineer, Aerosciences and Flight Mechanics, 2224 Bay Area Blvd, Houston TX, non-member.

N_c = Number of parachutes in a cluster

$\bar{q}$, qbar = Dynamic pressure, $\bar{q} = \frac{1}{2} \cdot \rho \cdot V_{air}^{\ 2}$

ρ, rho = Humidity-corrected atmospheric density

RC = Ramp Clear (usually chosen as start of test)

SAR = System Acceptance Review

σ, sigma = Standard deviation (general)

S/N = Serial Number

S_o = Parachute canopy full open reference area based on constructed shape including vents and slots

t_f = Canopy fill time from either bag strip or disreef to completion of stage inflation

t_i = Inflation start time of either bag strip or the disreef event from a previous stage

V_{air} = Total airspeed relative to air mass

V_i = Velocity (airspeed) at beginning of each stage at time t_i

W_p = Dry weight of parachute

I. Introduction

MODELS describing the Capsule Parachute Assembly System (CPAS) for the Orion/Multi-Purpose Crew Vehicle (MPCV) are documented in the "CPAS Model Memo." Version 18 of the Model Memo[1] supported CPAS System Acceptance Review (SAR) in 2019. Some potential improvements in the modeling methodologies were introduced when the models were adapted for similar Commercial Crew Program (CCP) parachute systems. This paper describes updates which are being retroactively applied to support modeling Artemis missions.

CPAS models of Forward Bay Cover Parachutes (FBCPs), drogues, and pilots were adequate for modeling analogous CCP parachute types. The only necessary update for drogues was to the reefing cutter timing model. A more complicated model was developed superimposing global temperature effects to in-lot cutter-to-cutter dispersions. This new model was also applied to the main parachutes and is described in Section II.

Most of the model improvements were to better predict margins on the main parachutes. Inaccuracies were discovered in the predictions of individual peak riser loads as well as the distributions of dispersed results.

Finite mass inflation model parameters are based on reconstructions of CPAS flight tests, as documented in Ref. 2. The typical reconstructions tended to emphasize matching the drag area history and overall trajectory of the test vehicle, sometimes at the expense of matching the magnitude of the peak inflation loads, as illustrated in Figure 1. Much of this can be attributed to known biases in the added mass model[3] currently included in the Flight Analysis and Simulation Tool (FAST). To make the model more precise, CPAS flight tests were re-reconstructed using search algorithms with FAST "in-the-loop" to better match peak loads (Section III).

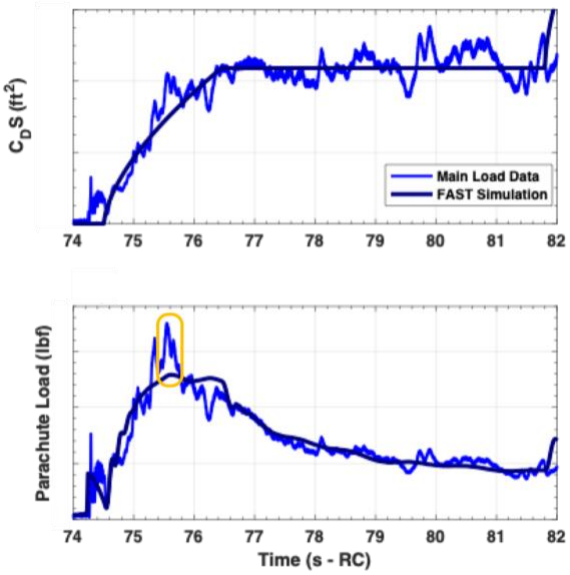

Figure 1. Typical individual CPAS main parachute reconstruction which optimizes drag area fit (top) but misses peak load (bottom).

A statistical analysis of Monte Carlo[4] results showed an under-representation of rare but possible main loads to the point that observed flight test experiences could not be replicated. The method of using independent (or uncorrelated) continuous probability density functions[5] was determined to sometimes produce non-physical combinations of inflation parameters. A method of drawing as-flown parameters combinations ("sampling") with some random noise injected ("jitter") was developed to make Monte Carlo results closer reflect the test campaign. The "sample/jitter" method is described in Section IV.

In order to quickly evaluate updated dispersed inputs, a "postflight Monte Carlo" technique was performed, as documented in Section V. Starting with a reconstruction of a particular flight test, dispersed inflation parameters are input for each stage, holding day-of-test variables constant. It is essential that the dispersed model should encompass

the observed loads, with a reasonable margin of alternate possibilities. After successful evaluation, the revised inputs were released internally as Model Memo version 18E.

II. Reefing Cutter Model Update

As of Model Memo v18, CPAS modeled reefing cutter dispersions based on distributions from video observations of 172 disreef events during flight testing. Each parachute in a given simulation had an uncorrelated dispersed scale factor applied. Because these flight tests were conducted throughout the year, temperature effects were not isolated. The resulting disreef loads from Monte Carlo simulations were overly conservative because wide differences in disreef times could lead to wide differences in peak loads among individual parachutes.

It is well known that colder temperatures tend to increase the delay of a reefing cutter and hotter temperatures tend to decrease the cutter duration.[6] CPAS evaluated temperature effects as part of the ground-based Destructive Lot Acceptance Test (DLAT) for the reefing cutters. The wide distribution of the previous model is compared with DLAT data in Figure 2. Because most of the ground tests were conducted at room temperature, ambient distribution became the primary source of the updated model, resulting in much narrower cutter-to-cutter dispersions.

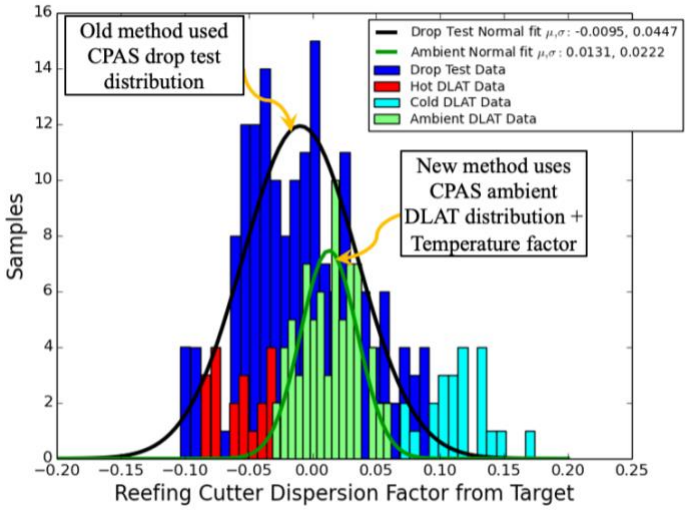

Figure 2. Model Memo v18 reefing cutter dispersion model based on flight test (dark blue) is much wider than ground test data at hot (red), ambient (green) and cold (cyan) conditions.

The updated algorithm is illustrated in Figure 3. First, temperature dispersion factors are drawn from a random uniform distribution of ±10%, which is on the order of the variation from ambient DLAT to the hot and cold dispersions. Each parachute has redundant reefing cutters, so random distributions are drawn for each reefing stage for each simulated parachute. The random dispersions use ambient DLAT normal distribution parameters and re-draw any cases beyond ±10% to reduce excessive tails. The temperature and in-lot dispersions are added together. For each reefing cutter pair, only the cutter with the shortest dispersed time is selected for the final distribution, which will therefore be slightly skewed.

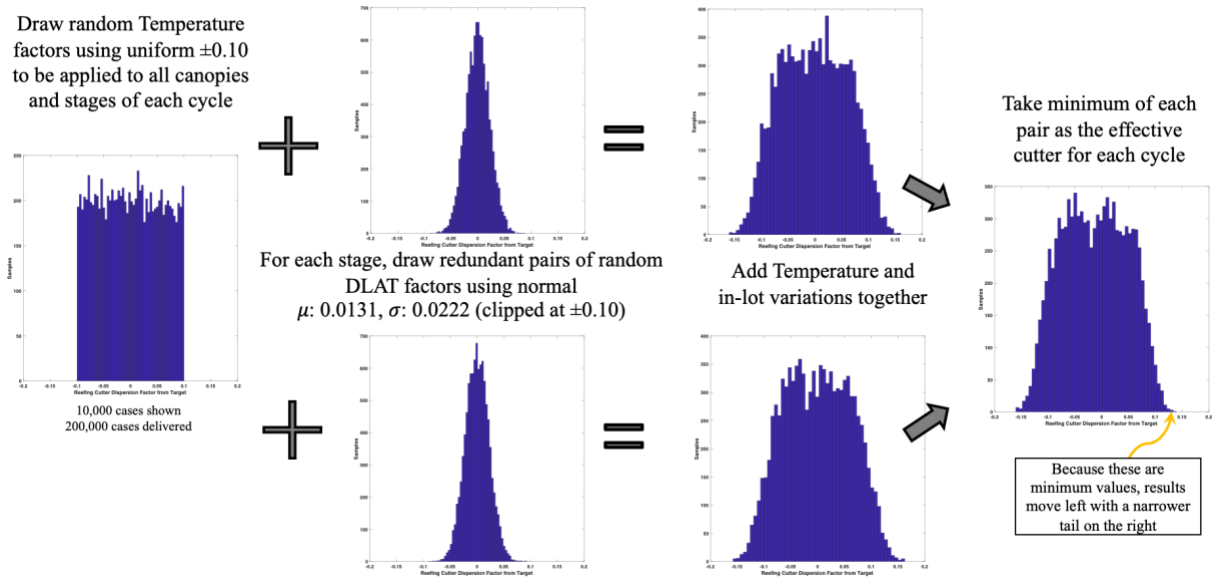

Figure 3. Updated CPAS reefing cutter dispersion algorithm. Temperature effects are superimposed with in-lot variation, as well as logic to simulate redundant cutters.

Dispersed output from the updated model for the first ten Monte Carlo cycles is shown in Figure 4. Because the temperature dispersion is applied uniformly to all cutters and parachutes in the given cycle, they will tend to run early or late together. This reduces the conservatism in parachute lead-lag while maintaining the overall width of temperature-induced dispersions. In fact, the same random number seed is used for the drogue parachutes, so a full system simulation will be consistent for the entire flight.

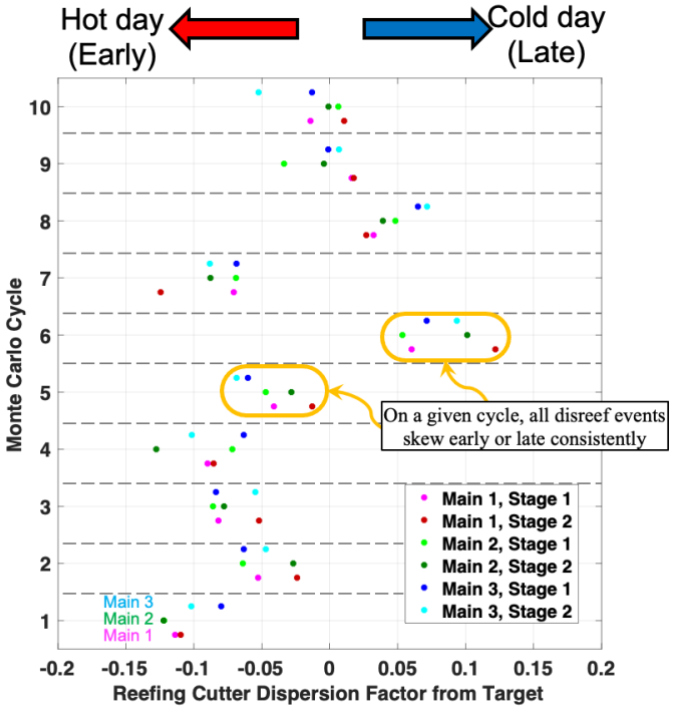

Figure 4. CPAS per-cycle reefing cutter model dispersed inputs for main parachutes.

III. Main Parachute Revised Reconstructions

The previous reconstruction technique for main parachutes involved matching the drag area growth curves for individual parachutes. Drag area data is approximated from the individual riser load, F_i, and parachute dry mass acceleration load factor, G, according to Eq. 1. Added mass and elastic spring effects are not estimated for "offline" data analysis, but are included in the reconstructed model. For that reason, even an excellent match of drag area growth may not result in a match of simulated peak loads.

$$(C_D S)_{p,i} \approx \frac{F_i + W_{p,i} \cdot G}{\bar{q}_\infty} \tag{1}$$

The drag area growth, $(C_D S)(t)$, is traditionally modeled using the power law in Eq. 2. The shape term, expopen, defines whether the growth is linear (= 1.0), concave up (> 1.0), or concave down (< 1.0). While this may describe the gross behavior over an entire stage, it does not have enough degrees of freedom to model changes in shape just after deployment or disreef, which has a large effect on the peak load.

$$(C_D S)(t) = (C_D S)_{i-1} + ((C_D S)_i - (C_D S)_{i-1}) \cdot \left(\frac{(t - t_i)}{t_f} \right)^{\text{expopen}} \tag{2}$$

The previous flight test reconstructions used search routines written in Python to adjust inflation parameters to exactly match peak loads for the infinite mass inflation CPAS parachutes (FBCPs and drogues). Because the added mass effects are computed in the simulation, the routine uses FAST "in-the-loop." The method was adapted to the finite mass main parachutes for Model Memo v18E. The fill constant, n, is adjusted iteratively to match a measured peak load. An example of this process applied to Cluster Qualification Test (CQT)-4-4 is shown in Figure 5. All three canopies in the original reconstruction (left) match the drag area growth data, but the simulated peak loads for two canopies are too low. For each canopy, it is possible to search for the fill constant that results in an exact match of the actual peak load. The reconstruction is complicated by the fact that adjusting the parameters of any parachute affects the whole system and causes other parachute load matches to diverge. It is helpful to optimize each parachute in order from fastest to slowest inflation to minimize downstream effects. Obtaining acceptable matches for the entire cluster requires applying the search routine over several iterations. The resulting reconstruction for this case (right) matches the peak loads within a certain tolerance by reducing the fill constants by as much as 77%. The faster-than-actual simulated inflation times results in an earlier application of drag, such that the inflated drag areas are each reduced by 11% to compensate.

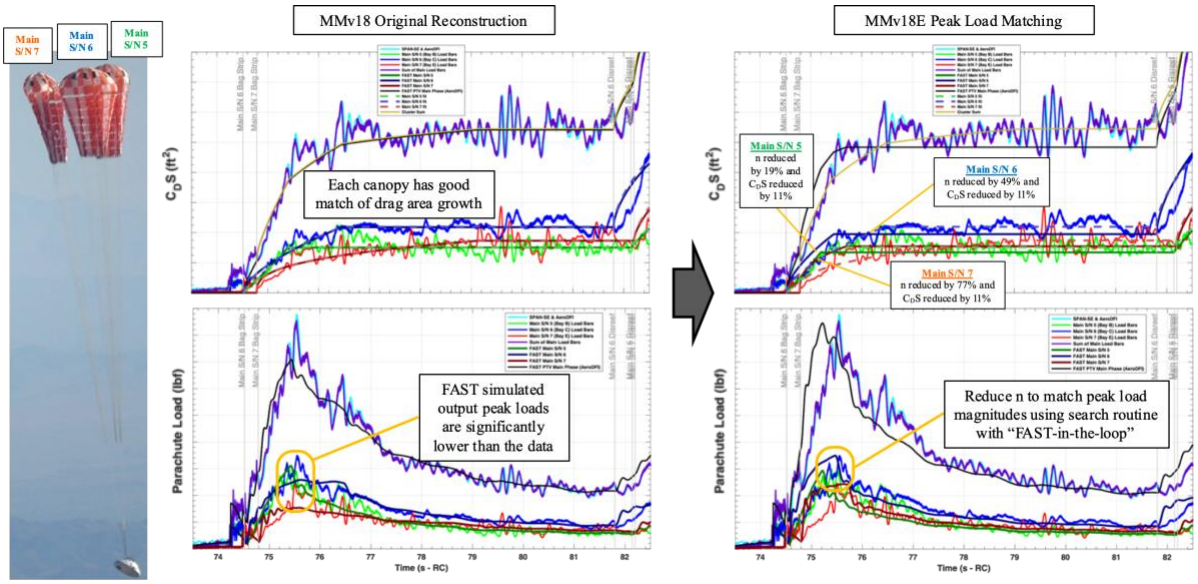

Figure 5. CQT-4-4 main first stage FAST-In-The-Loop re-reconstruction. The fill constants are reduced using a search algorithm to match the exact measured peak load for each canopy.

The reason for the drag area reduction is illustrated by trajectory matching in Figure 6. The original reconstruction (left) had adjusted the cluster drag such that the simulation exactly matched the actual altitude at the end of the stage. Reducing the fill constants to match inflation loads decelerated the system faster and resulted in exceeding the actual altitude by about 50 feet at disreef (center). This divergence from reality would reduce the accuracy of reconstructions for subsequent stages. To compensate, another search routine was applied to determine the amount of drag reduction necessary to match the altitude (right). However, this caused the simulated dynamic pressure to diverge from the data. It is not possible to simultaneously match the inflation loads, altitude, and dynamic pressure without a revising the added mass model to match inflation timing. In the future, NASA may consider modeling each physical stage as two sub-stages. This would allow for isolating an optimized match of the peak load in the first sub-stage and matching the trajectory by adjusting the second sub-stage drag area. The tradeoff for higher fidelity simulations is additional degrees of freedom to be dispersed.

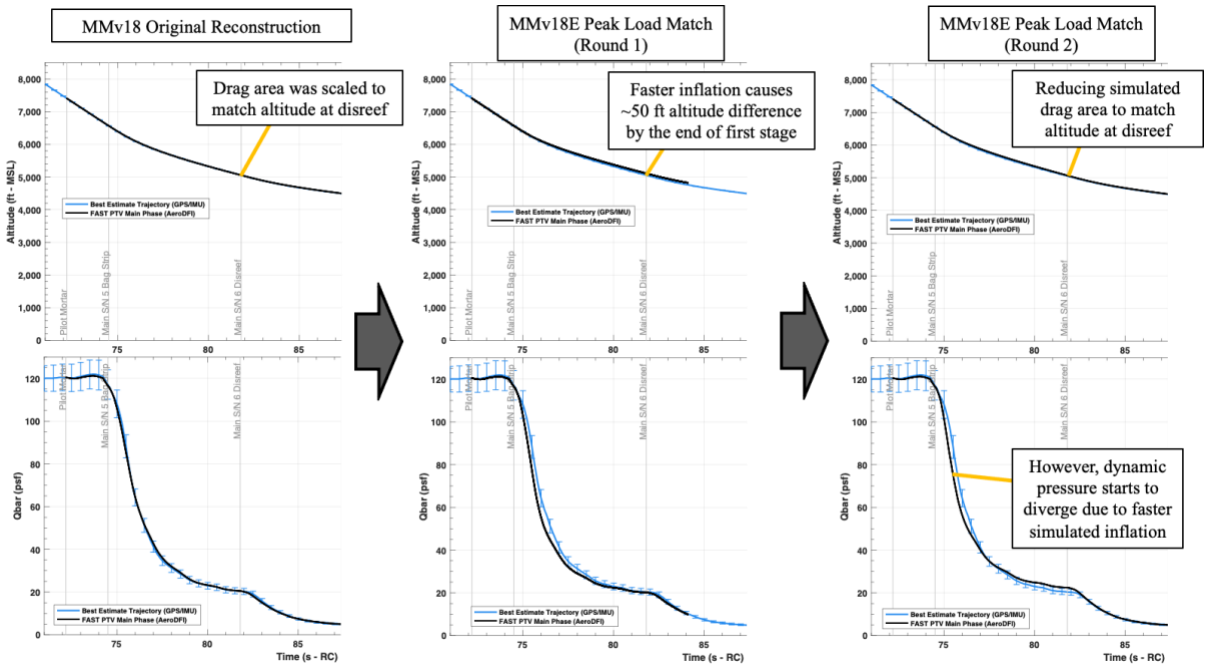

Figure 6. CQT-4-4 main first stage loads matching causes a divergence in matching the trajectory.

Figure 7 shows how the process can match a second stage disreef load for Cluster Development Test (CDT)-3-15. The original reconstruction output peak load was significantly lower than the data for the dominant canopy (S/N 14). A loads match was only attempted on the dominant parachute for this case, which was much more straightforward than for multiple canopies in the previous example. There is a minimum of one round of iteration to scale the ending drag area to match the altitude, and then re-compute the necessary fill constant to match the peak load with the new drag area.

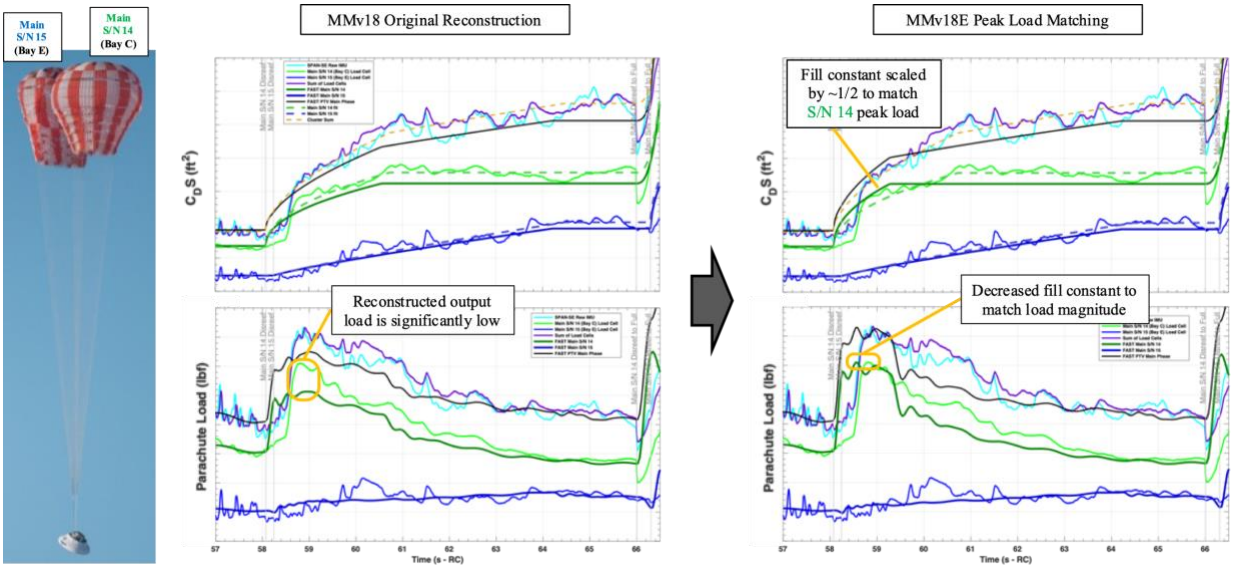

Figure 7. CDT-3-15 main second stage FAST-In-The-Loop re-reconstruction. The fill constant is reduced using a search algorithm to match the exact measured peak load.

Many CPAS reconstructions for Model Memo v18 had peak loads within 5% of the data and were therefore considered acceptable. A total of eleven CPAS tests were reconstructed using the above method to match loads for Model Memo v18E.

IV. Main Parachute Sample/Jitter Dispersed Inputs

Early CPAS models of main inflation dispersed the three primary parameters independently, often resulting in non-physical combinations. To compensate, the fill constant and exponential terms were plotted in two dimensions and bounded using the MATLAB convex hull algorithm ("convhull"), as if restricted by a rubber band. This 2-D formulation is shown in the left of Figure 8. After CPAS SAR, analysis showed another strong correlation, this time between fill constant and drag area. Tests that inflate over a short distance tended to end up with lower drag areas. In other words, there should be a minimum fill distance for a given ending drag area. Yet certain Monte Carlo combinations of small fill constants resulting in high drag areas were leading to overly conservative loads. Considering these observations, Model Memo v18A expanded the convex hull algorithm to three dimensions, as if the points were wrapped in an elastic sheet, as shown on the right of the figure. This additional restriction was computationally expensive, and yet certain physically unlikely combinations still tended to get over-represented, while actual flight test points might never get included in the distributions.

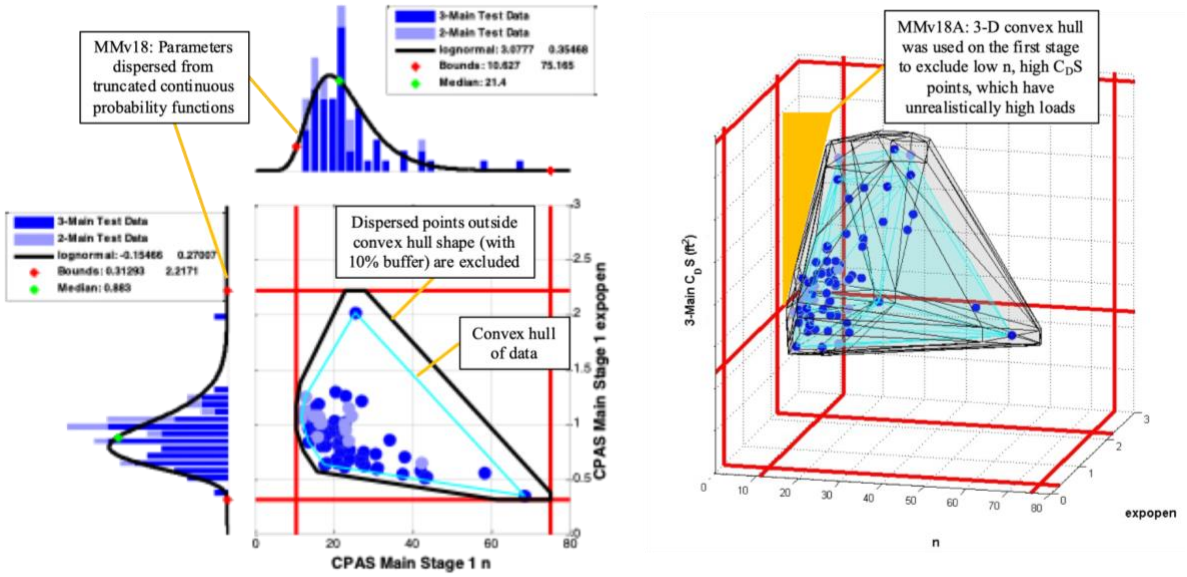

Figure 8. Main first stage 2-D convex hull method for continuous probability functions (left) and additional 3-D drag area restriction for Model Memo v18A (right).

An investigation showed that the method of modeling individual parameters as continuous probability density functions (truncated normal or lognormal) was the cause. Test points in a tail were under-represented, and points that are in multiple tails are almost never drawn. Therefore, the best way to reflect the relative probability of flight test occurrences was to draw from a database of reconstructed "samples" equally. Points from updated reconstructions of the first stage for clusters of three mains are shown in Figure 9. The combinations are best represented as 3-D points to reflect the interactions between parameters.

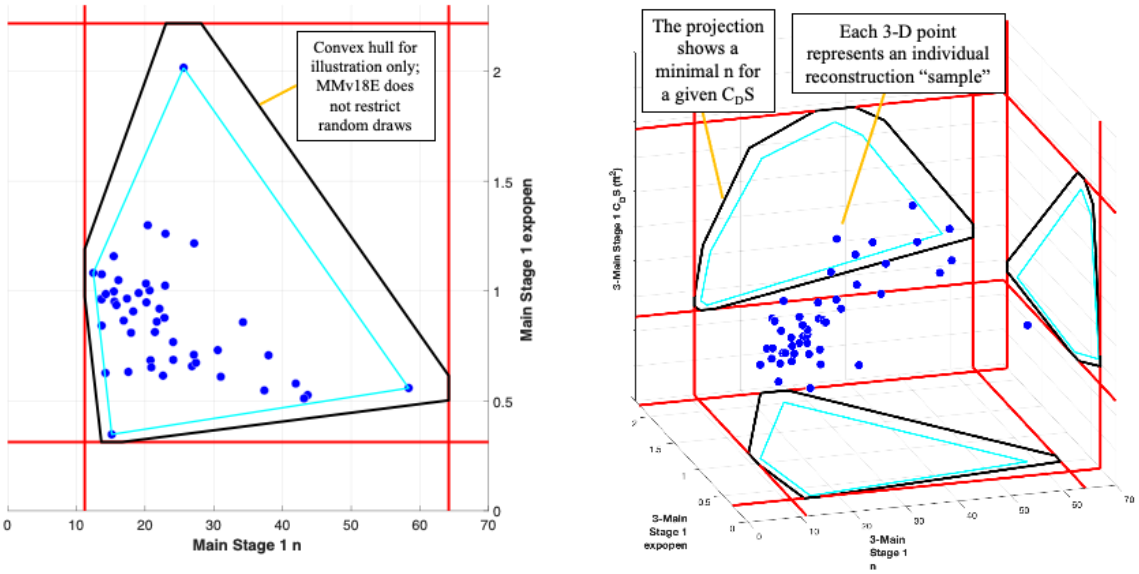

Figure 9. First stage reconstructed "samples" represent expected combinations of inflation parameters for tests with three mains.

Knowing that test data had measurement uncertainties and the reconstruction techniques had additional errors, it was necessary to apply some random "jitter" to these samples, as shown in Figure 10. Point clouds are generated around each reconstructed point using normal distributions with standard deviation scaled such that 3σ matched an Engineering Factor (EF) of either 10% for n and expopen, or 5% for drag area. The EF is also intended to cover for the limited number of flight tests. It seems unlikely that the worst possible conditions have already been encountered.

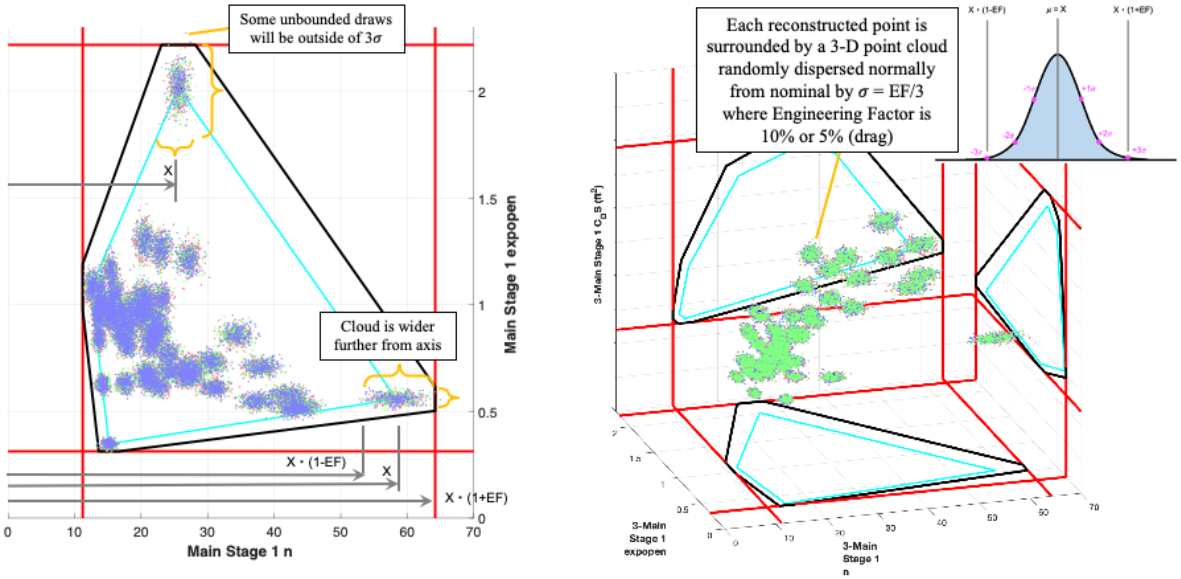

Figure 10. Main first stage parameters with probabilistic "jitter" point clouds for Monte Carlo inputs.

One potential disadvantage of the sample/jitter method is the loss of statistical significance by segregating according to number of mains in a cluster (N_c). It has been shown that individual drag area tends to be more efficient in clusters of two (a single-failure mode) than in clusters of three (nominal configuration). While the previous method grouped reconstructed points in 2-D space regardless of cluster size, the additional drag area dimension prevents grouping in the sample-jitter method. Because most of the flight campaign was for the nominal configuration, about

2/3 of the reconstructed data are used for modeling three-main cases and only about 1/3 of the reconstructed data are used for modeling two-main cases.

Histograms of the dispersed Monte Carlo inputs for first stage clusters are compared in Figure 11. On the upper left, draws from MMv18 are concentrated in high-probability regions, which tend to exaggerate peak loads. Meanwhile, many draws are distributed along the upper right edge of the convex hull, which has never been observed in flight (and will later be shown to be impossible). Yet some actual flight test points with large fill constants have no probability of ever being drawn. It is important to include lagging inflations to accurately predict the risk of altitude loss. The sample/jitter method for MMv18E draws individual test points with the same probability as occurred in flight. The three-main cases on the upper right cover about the same probability space as the old method, but the two-main cases on the lower left have a smaller probability space. This may be due to the lower number of two-main flights or may reflect some physical restriction to interactions with fewer canopies.

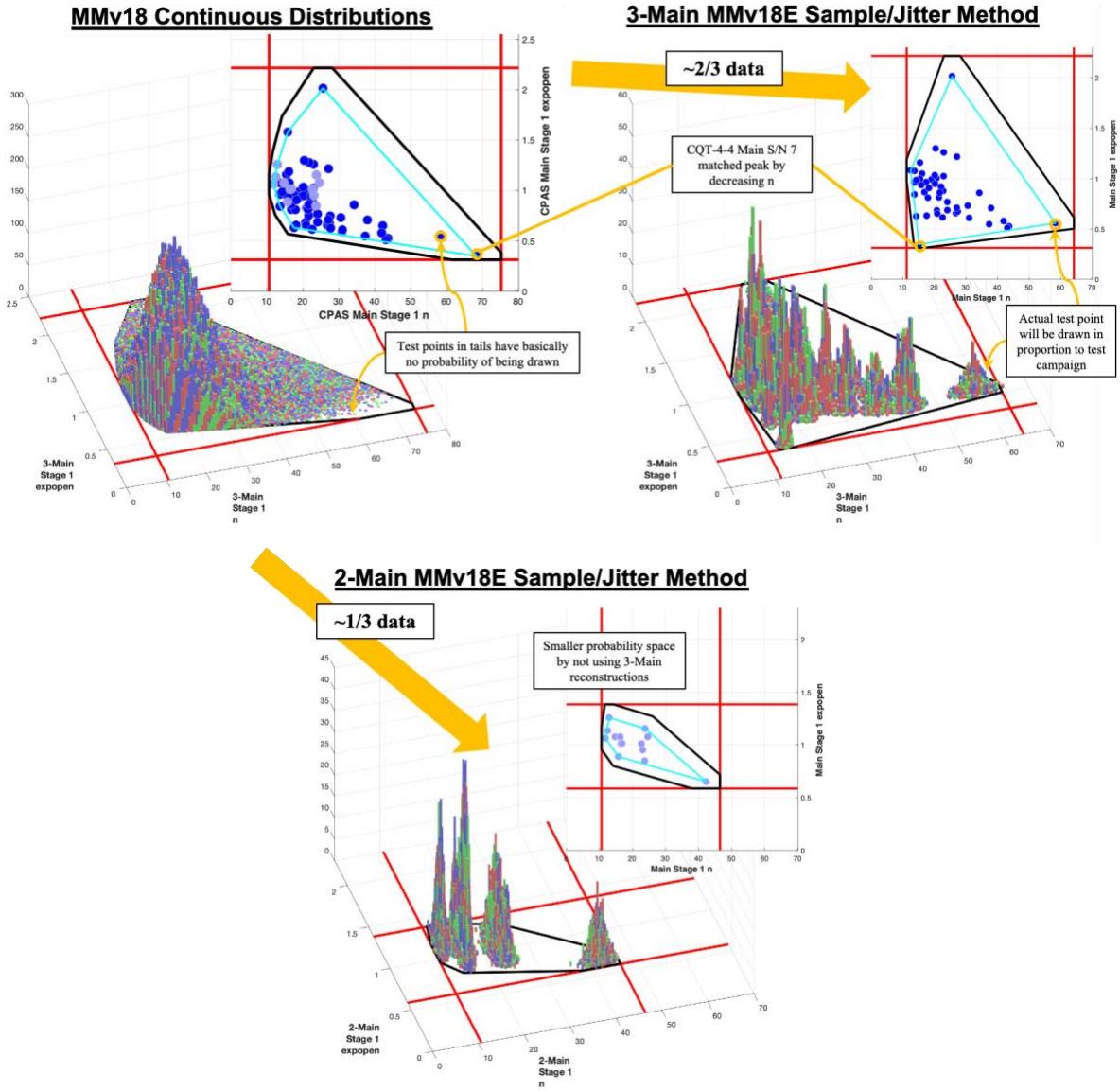

Figure 11. First stage dispersed Monte Carlo inputs comparing MMv18 to MMv18E. Parameters using the sample/jitter method are correlated and will be more representative of flight test experience.

To better understand the relationship between the 3-D inflation parameter and physical inflations, an effort was made to determine reasonable inflation profiles within flight test experience. Figure 12 shows the 3-D points

representing reconstructed flight tests on the left. Eight points based beyond the extreme test points define a boundary box. The geometric centroid is considered the nominal inflation. Time histories of all the reconstructed test points (assuming identical initial conditions) are plotted in blue on the right of the figure. The bounding envelope of the reconstructed inflations is drawn in green. The nominal inflation parameters have a time history centered within the envelope. However, the eight red curves are based on the boundary box points and mostly have time histories that fall far outside flight test experience, which would result in either extremely high or low simulated loads. This reinforces the decision to use a sampling method to avoid simulating these extreme cases.

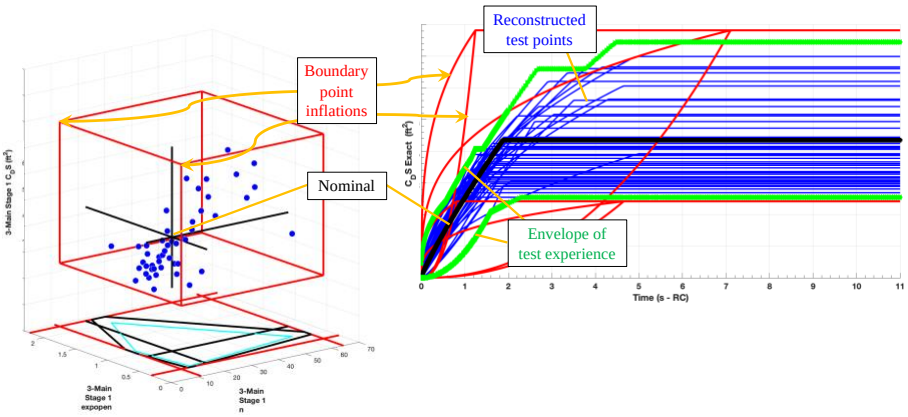

Figure 12. Range of inflation test experience.

Figure 13 shows a grid search conducted throughout the 3-D parameters space. For each candidate point, the corresponding drag area time history was generated, as shown on the right. Candidate points with time histories within the test experience envelope were retained and plotted and points outside test experience were rejected. The resulting map of physically reasonable inflations provides some insights. The 2-D map (center) shows many points with small fill constants, even lower than the Engineering Factor bound. Fast inflations from low fill constants tend to create high loads. However, it can be seen in 3-D (left) that these fast inflations are associated with very low drag areas, which result in low loads. This confirms the relationship of minimal fill constant for a given ending drag area which was enforced since Model Memo v18A. A large region of high fill constant and high expopen which was simulated in MMv18 is basically not possible. There is a large space of theoretical inflations with very large fill constants, potentially stretching to infinity. However, these should be truncated by the temporal constraint of the 8-second disreef cutter.

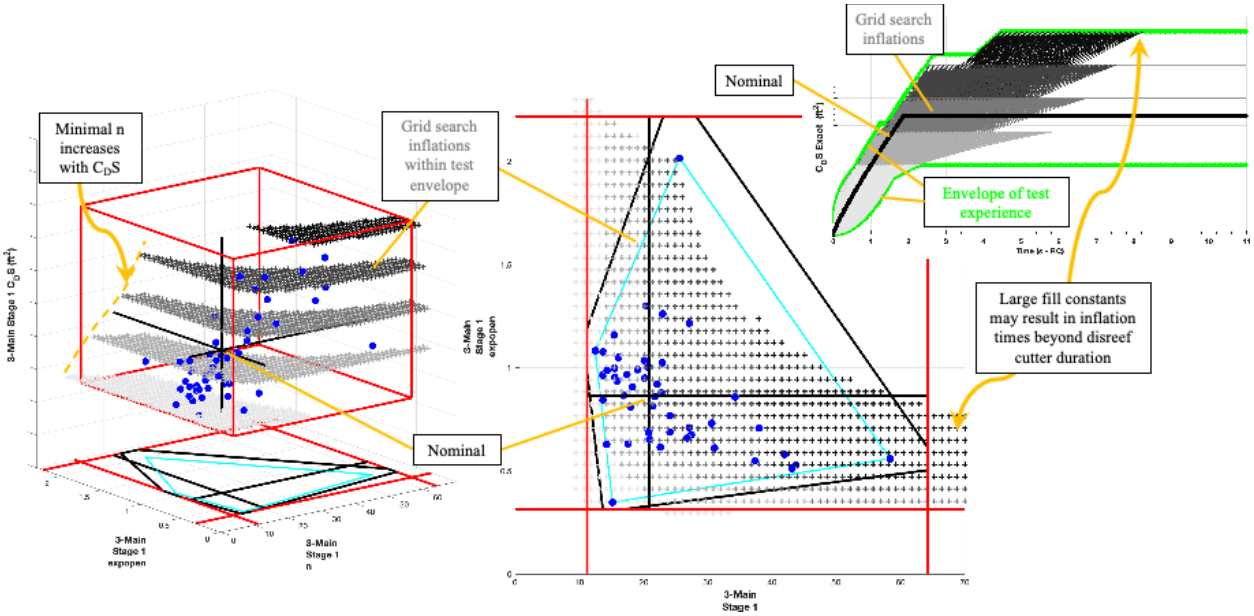

Figure 13. Grid search of inflation parameters resulting in profiles within test experience.

The grid search is limited in that while it may show which combinations are possible, it does not indicate the relative probability of occurrence. Further investigation of the parameter space may continue in the future, such as combining it with multivariate density functions. However, the sample/jitter method has the advantage of low computational cost and should best reflect relative frequency, assuming a sufficiently large number of test points.

The relationship between fill constant and drag area observed in first stage also holds for other stages. It gets more complicated because the relevant metric is the change is drag area from stage to stage. Model Memo v18 dispersed each stage independently, so a parachute might get simulated with a very low random drag area in one stage and a very high drag in the next, which tended not to occur in flight, and may not be physically possible for a particular random fill constant. Therefore, each "sample" was chosen to represent the entire set of conditions for all three stages from a given individual parachute reconstruction. This helps limit the potential Monte Carlo space for a given simulated parachute.

The versions of dispersed input releases between MMv18B and MMv18E worked out some details of the dispersion methods. At one time the "jitter" was limited to prevent dispersions beyond the Engineering Factor, but the few cases beyond 3σ had little effect on the Monte Carlo results. Another question regarded how to treat the dependence on the main deployment bay. Despite all pilot mortars firing simultaneously, main parachutes tend to deploy from Orion with slight timing differences based on the hang angle under the drogues. Bays B and E tend to get to bag strip before Bay C, because the corresponding pilot from Bay D gets mortared into the airstream and takes a longer deployment path. To maintain a strict adherence to flight experience, Monte Carlo draws from each bay would only be drawn from tests points obtained from corresponding locations. This would tend to limit the Monte Carlo simulations to repeating the test campaign with little variation. Eventually, it was decided to allow for randomizing test points such that that they could be assigned to any bay. This also allows a particular test point to be repeated within a cluster on the same cycle. This was seen as a good compromise to allow for cluster combinations not seen in flight without straying too far outside experience. Random "all leader" and "all lagger" draws tend to result in moderate to low parachute loads, while wide divergences in parameters cause high loads on the "leader" canopy. Further studies of purposely assigning leading and lagging combinations have been examined for CCP, but have not yet been incorporated into Orion distributions.

V. Postflight Monte Carlo Verification

The postflight Monte Carlo method (described by E. Hultgren of SpaceX as the "*a posteriori* simulation" method) is a technique to evaluate dispersed inputs on a baseline flight test reconstruction. The initial flight reconstruction should be tailored to match peak inflation loads in each stage (Section II). The process is outlined in Figure 14. Day-of-flight conditions such as atmosphere, initial state, mass properties, and disreef timing are held constant. Only inflation parameters are varied, based on the model input files being evaluated. To prevent dispersions of early stages from "bleeding into" later stages, the simulation should be split into multiple pieces. The first piece is only evaluated until the first disreef event. The second piece uses undispersed reconstructed inflation parameters until disreef to second stage, and so on.

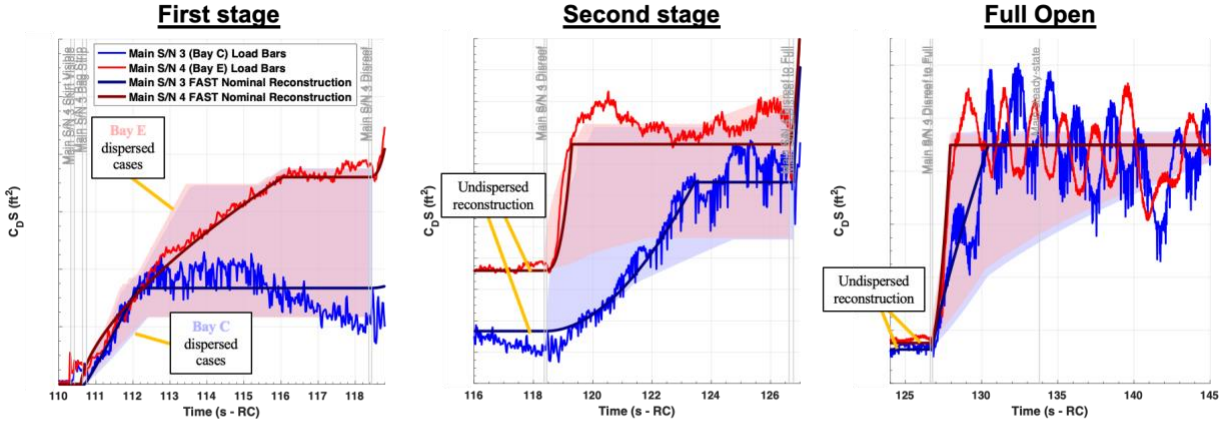

- Initial conditions, atmosphere, disreef timing, etc. are based on day-of-flight *a posteriori* data
- Only the first stage inflation parameters are dispersed from Monte Carlo input files
- Undispersed reconstructed parameters are used for first stage
- Match nominal trajectory through disreef to second stage
- Second stage inflation parameters are dispersed
- Undispersed reconstructed parameters are used for first & second stage
- Match nominal trajectory through disreef to full open
- Full open inflation parameters are dispersed

Figure 14. Postflight Monte Carlo methodology to isolate stage loads.

A. First Stage Postflight Monte Carlo Example

An example of a postflight reconstruction for the first stage of CDT-3-15 is shown in Figure 15. The actual measured peak loads (dashed vertical red lines) are contained within the dispersed output histograms. Previously, the Main S/N 14 peak load was in only in the 88th percentile of the Model Memo v18 output. This long tail to the right was overly conservative, because the high measured drag (and therefore load) on S/N 14 was the fleet leader from flight test, and therefore should have been the limiting case approaching the upper bound. Using the Model Memo v18E inputs, the as-measured load is in the more reasonable 94th percentile.

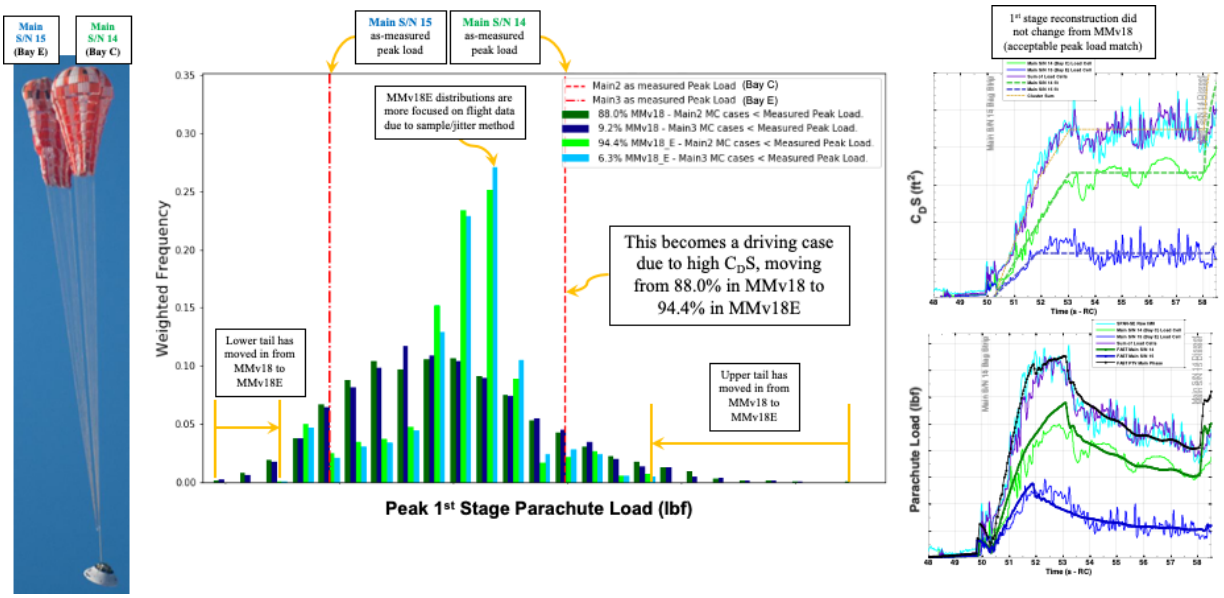

Figure 15. Postflight reconstruction of CDT-3-15 first stage. The overly conservative long tails from MMv18 have been brought to more reasonable limits with MMv18E.

B. Second Stage Postflight Monte Carlo Drivers

A driving case for second stage Monte Carlo loads is the reconstruction of a "snappy" inflation by Main S/N 4 on CQT-4-3. The reconstruction was improved by matching the peak load as shown in Figure 16. Yet the inflation parameters are still fast and highly concave-up with a low fill constant and high exponential term.

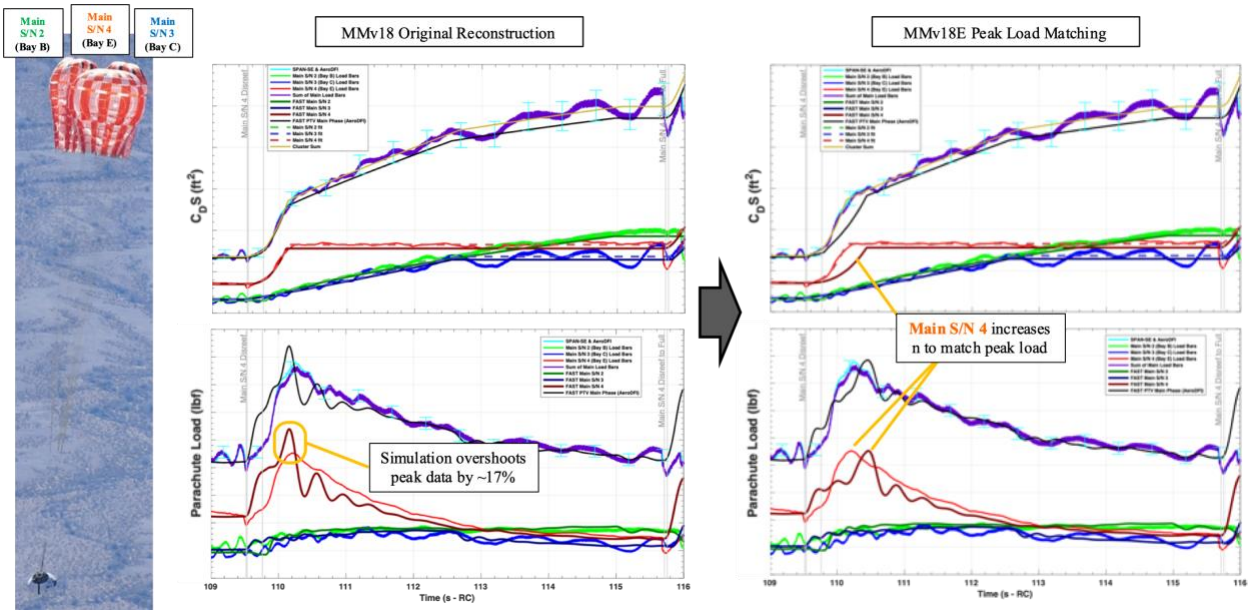

Figure 16. CQT-4-3 main second stage FAST-In-The-Loop re-reconstruction of leading main S/N 4.

Postflight reconstruction for this case is shown in Figure 17. Using the MMv18 dispersions, the as-measured peak load from S/N 4 was in the 99.9th percentile, meaning it was basically the highest load in all the Monte Carlo simulations for this stage. One would expect the possibility of higher loads, had more tests been conducted. The MMv18E dispersions expanded the upper tail such that the observed load was lowered to the 98.5th percentile.

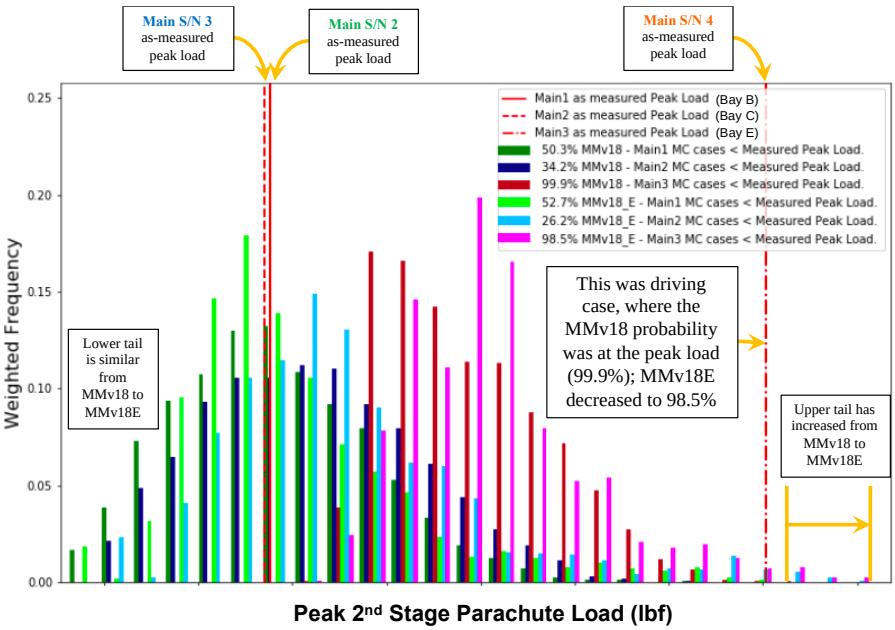

Figure 17. Postflight reconstruction of CQT-4-3 second stage. The as-measured peak load from S/N 4 was at the extreme end of the MMv18

An explanation of the distributions can be seen in Figure 18. A histogram of the MMv18 inputs show very few draws in the region associated with fast disreef inflations. In fact, the center plot shows three reconstructed samples in that region. Therefore, the sample/jitter method of MMv18E will better represent the relative probabilities of those occurrences, improving the accuracy of loads predictions and margins analysis.

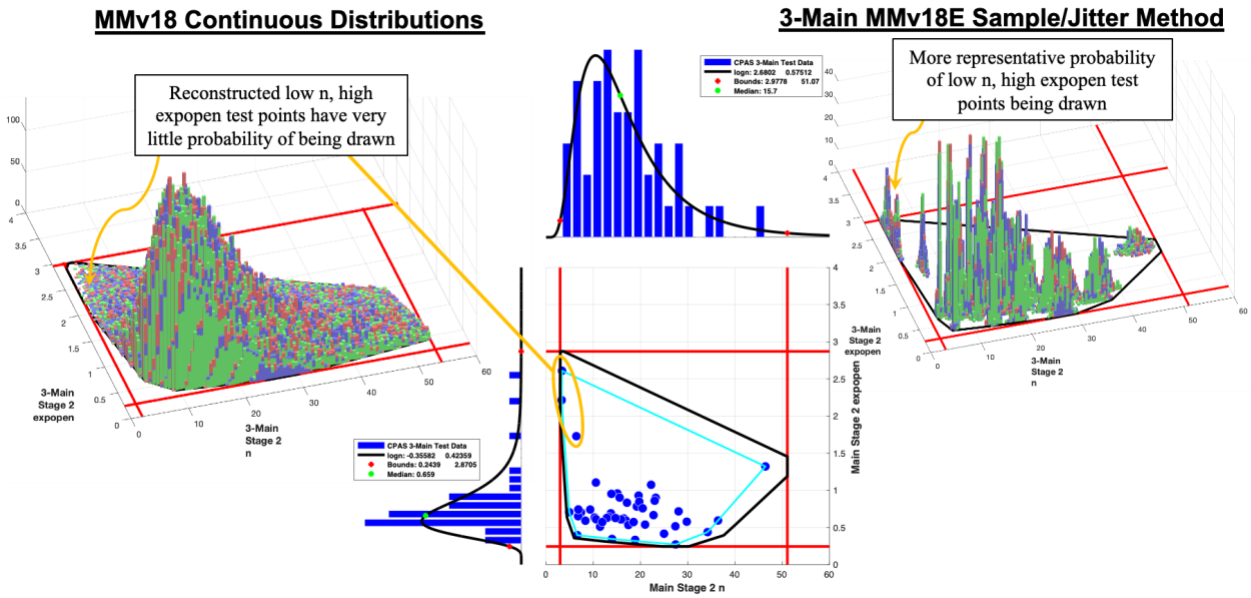

Figure 18. Three-main second stage dispersed Monte Carlo inputs comparing MMv18 to MMv18E. Some flight test points associated with high disreef loads had poor representation using continuous distributions.

A similar situation occurs in the two-main configuration. The driving case for the second stage Monte Carlo loads originates with Main S/N 4 on CQT-4-5. It too had a highly concave-up, fast inflation. The postflight Monte Carlo results for that test are shown in Figure 19. The as-measured peak load is still at the extreme end of the updated Monte Carlo distribution, probably because of the relatively low number of two-main flight tests.

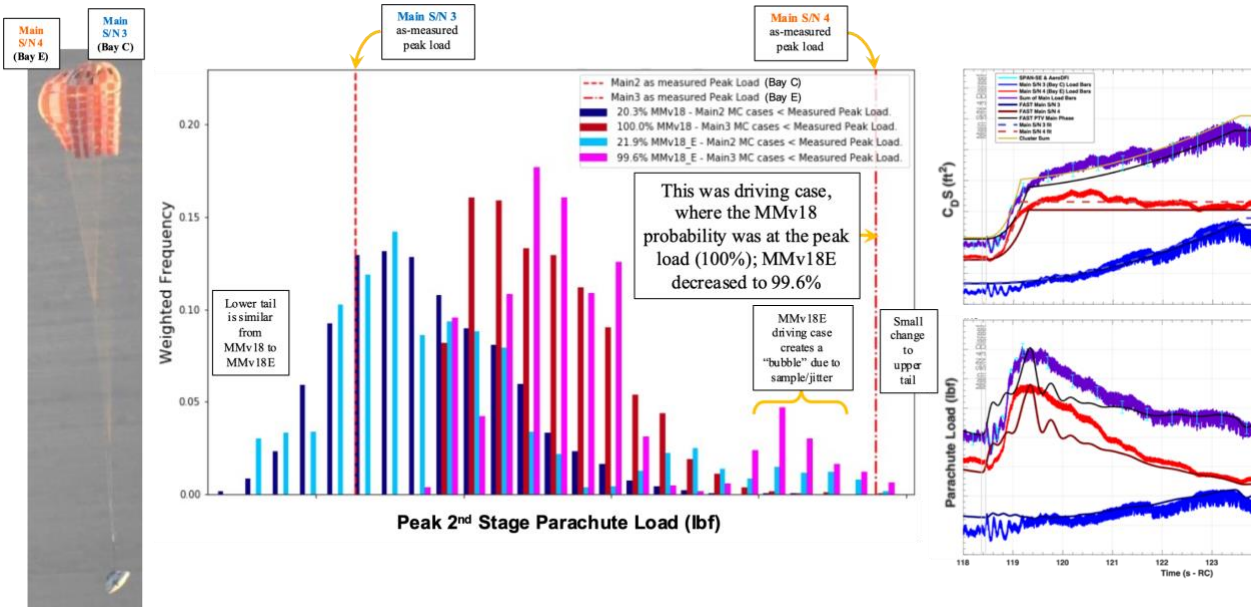

Figure 19. Postflight reconstruction of CQT-4-5 second stage. This is still the driving case, but has moved from the 100th percentile in MMv18 to the 99.6th percentile in MMv18E.

Another extreme two-main lead-lag disreef event occurred on CDT-3-15. In this case, the leading main (S/N 14) had a concave-down inflation. The updated reconstruction from CDT-3-15 S/N 14 had reduced its fill constant by about half to better match the as-measured peak load. The postflight Monte Carlo study in Figure 20 shows a much larger effect of the sample/jitter method on the location of the as-measured peak load, reducing it from the 99.8th percentile to the 91.9th percentile, showing the updated Monte Carlo distribution is more conservative with a larger buffer.

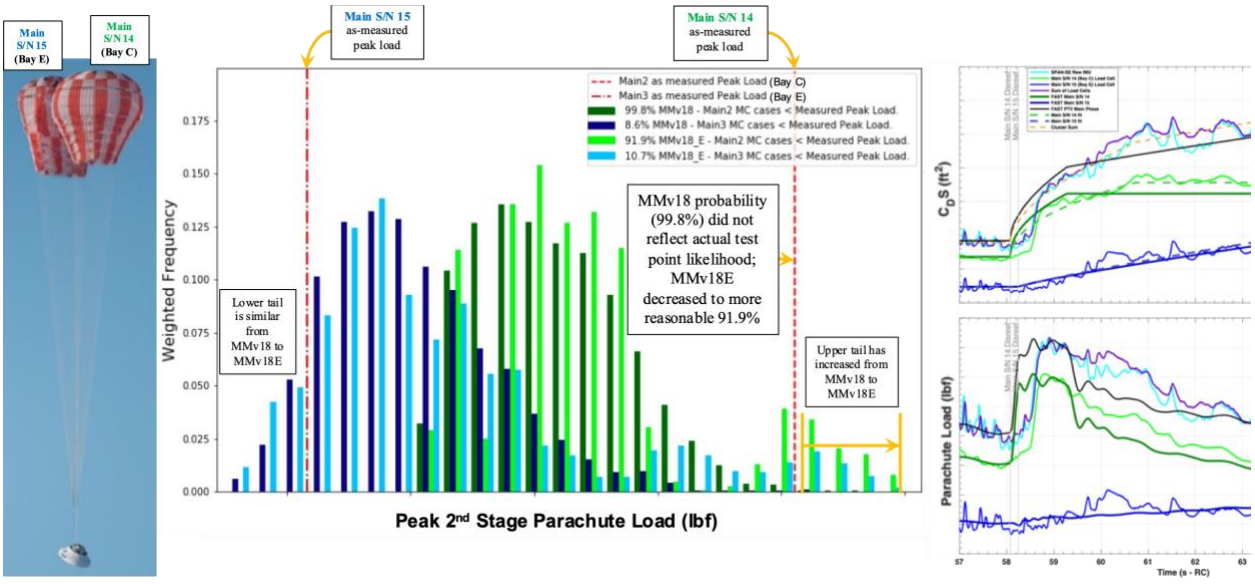

Figure 20. Postflight reconstruction of CDT-3-15 second stage. Main S/N 14 has been reduced from the 99.8th percentile in MMv18 to a more reasonable 91.9th percentile in MMv18E.

Dispersed input histograms from both versions are compared in Figure 21. As with the three-main configuration, the driving case previously had very little probability of being drawn. MMv18E has noticeable gaps between reconstructed points due to the limited number of two-main reconstructions.

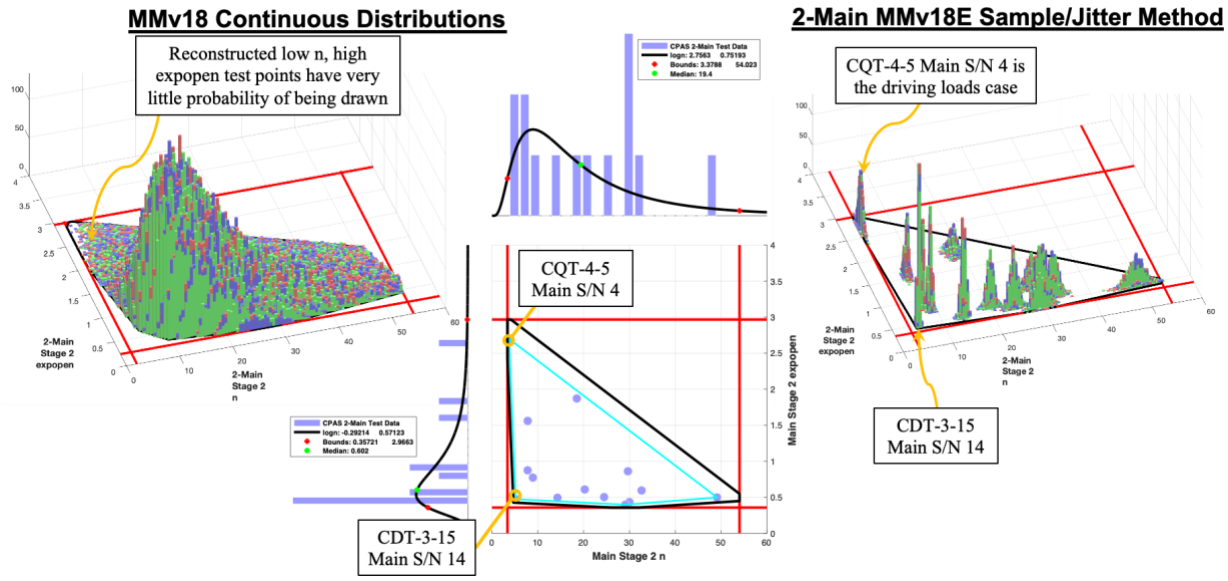

Figure 21. Two-main second stage dispersed Monte Carlo inputs comparing MMv18 to MMv18E. The previously discussed example test points are identified.

C. Full Open Postflight Monte Carlo Drivers

Like second stage, disreef loads to full open tended to be driven by canopies that were larger at the end of a stage, disreefed earliest, and took advantage of lower interference to inflate quickly. Main S/N 7 on CDT-3-17 was just such a strong leader. As seen in Figure 22, the corresponding reconstructed point was in a low-probability region for MMv18, so the Monte Carlo results may not have been conservative. That point is drawn much more often with the sample/jitter method.

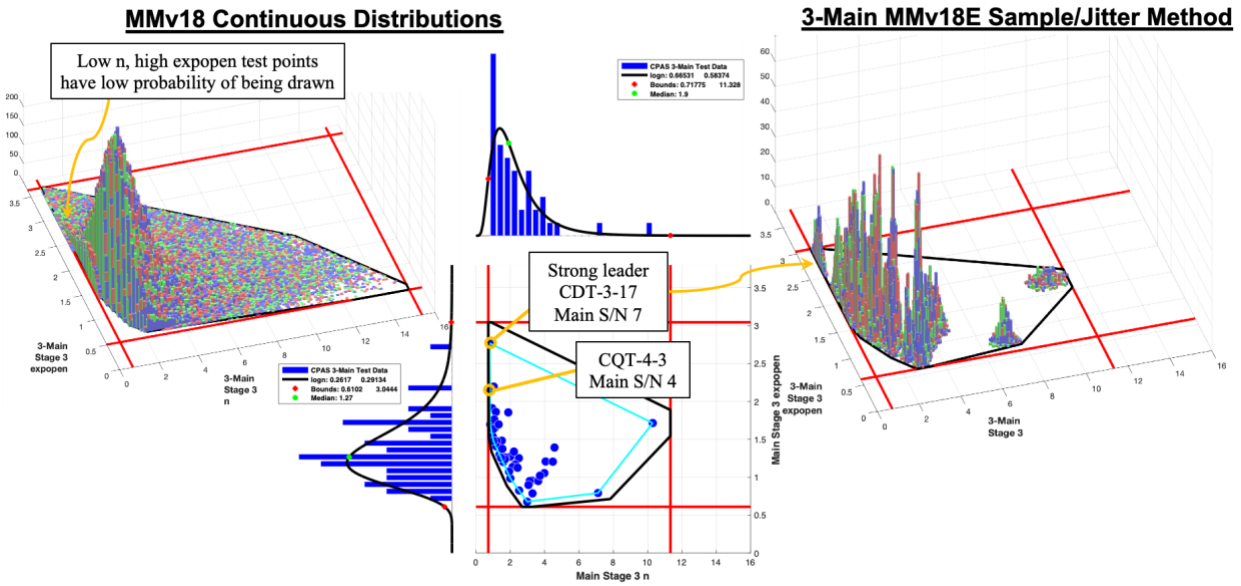

Figure 22. Three-main full open dispersed Monte Carlo inputs comparing MMv18 to MMv18E.

A similar full open "super-leader" for the two-main configuration was main S/N 14 on CDT-3-15, where the postflight Monte Carlo study is shown in Figure 23. The probability for the as-measured peak load only changed about 1% between versions, but the histogram for MMv18E shows a "bubble" at high loads not present in MMv18, reflecting higher representation of that test point.

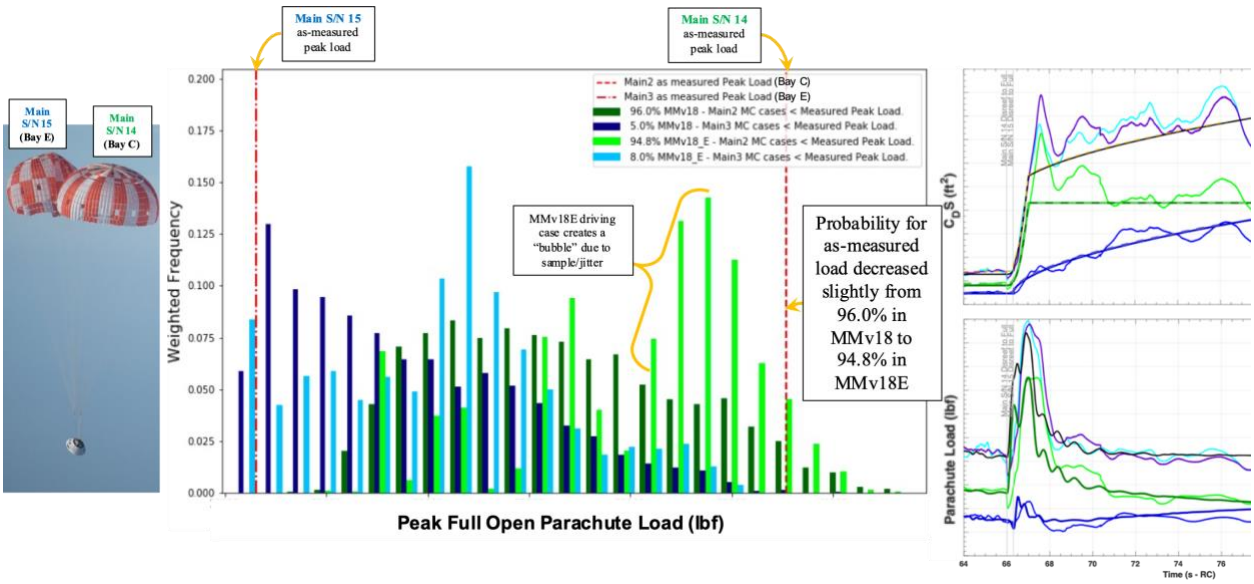

Figure 23. Postflight reconstruction of CDT-3-15 full open. Main S/N 14 probability was slightly reduced.

The reconstructed CDT-3-15 S/N 14 test point is labeled in Figure 24, showing the higher likelihood of drawing the "super-leader" case, and therefore making the simulation more conservative in loads. Another consideration at the other end of the spectrum is the higher representation of a "super-lagger" canopy, which is important to be conservative in estimating safe altitude margin.

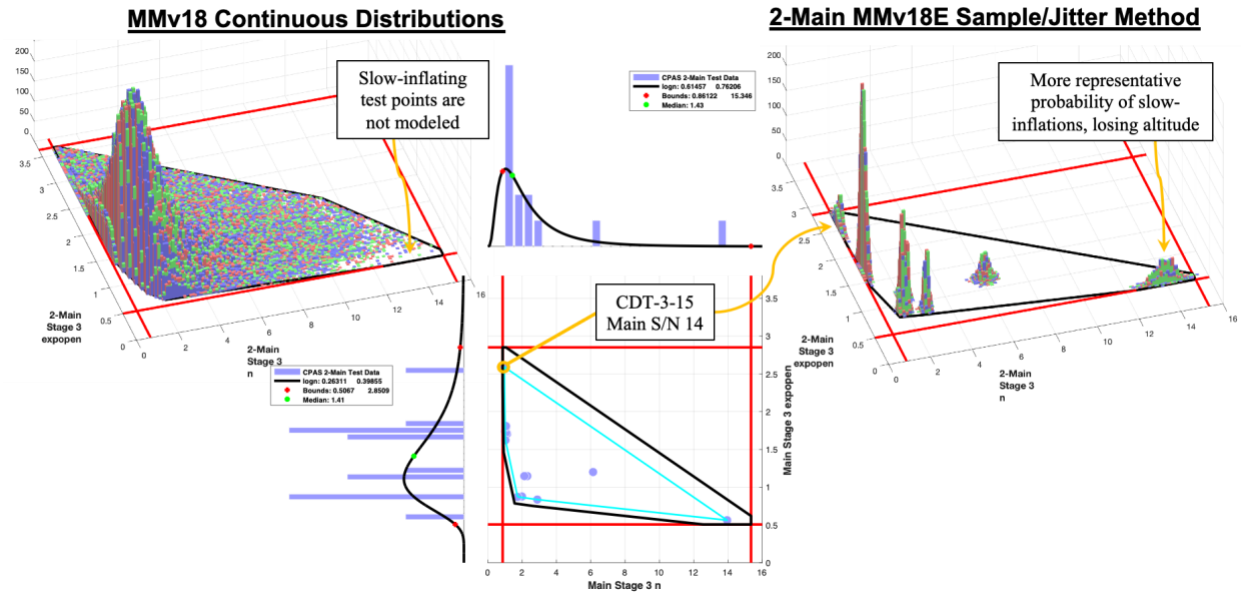

Figure 24. Two-main full open dispersed Monte Carlo inputs comparing MMv18 to MMv18E.

VI. Conclusion

The modeling of CPAS parachutes has been modified from the previous baseline at system certification to incorporating experience with similar CCP parachutes. The reefing cutter timing model now generates temperature variations to all cutters in a given simulation in addition to expected individual variation. This reduces the canopy-to-canopy disreef discrepancy which tended to exaggerate individual parachute loads. It still maintains the temperature effects that cause cutters to activate early or late, except now all the simulated cutters on a given Monte Carlo cycle will shift the same amount.

The largest effort to improve the model was focused on main parachute inflation. Uncorrelated continuous distribution functions were resulting in combined parameters that were not representative of actual occurrences from flight testing. A sample/jitter technique was developed by dispersing as-flown correlated parameters such that Monte Carlo inputs are more reflective of relative probabilities of inflation observed in flight.

Postflight Monte Carlo studies were conducted on several driving cases for each stage and cluster configuration. Nominal reconstructed input files were used as a baseline using day-of-flight conditions. The inflation parameters were then dispersed at each stage to and the dispersed output loads were compared with the as-measured loads. These studies were useful to help predict how Monte Carlo dispersions affect simulated parachutes under realistic conditions.

Acknowledgments

The authors wish to thank Peter A. Parker, Ph.D., P.E., of the NASA Engineering & Safety Center for consulting on statistical techniques.

References

[1] Ray, E. S., "*CPAS Operating Modeling Parameters Version 18 (System Acceptance Review)*," NASA JSC 65914 Rev. M, April 2019.

[2] Ray, E. S., "Updated Reconstruction Methods for Modeling Orion Parachute Loads," *25th AIAA Aerodynamic Decelerator Systems Technology Conference and Seminar*, Dallas, Texas, June 2019, AIAA paper 2019-3143.

[3] Ray, E. S., "Isolating Added Mass Load Components of CPAS Main Clusters," *24th AIAA Aerodynamic Decelerator Systems Technology Conference and Seminar*, Denver, Colorado, June 2017, AIAA paper 2017-3232.

[4]Moore, J. W., and Morris, A. L., "Development of Monte Carlo Capability for Orion Parachute Simulations," *21st AIAA Aerodynamics Decelerator Systems Technology Conference*, Dublin, Ireland, May 2011, AIAA paper 2011-2610.

[5] Romero, L. M. and Ray, E. S., "Application of Statistically Derived CPAS Parachute Parameters," *22nd AIAA Aerodynamic Decelerator Systems Technology Conference*, Daytona Beach, Florida, March 2013, AIAA paper 2013-1266.

[6] Barlog, S. J., "Practical Aspects of Reefing Cutter Design," *6th Aerodynamic Decelerator and Balloon Technology Conference*, Houston, TX, March 1979, AIAA Paper 1979-0418.